Asian Journal of Nanoscience and Materials 5 (2022) 196-210

SPC

Asian Journal of Nanoscience and Materials

Journal homepage: www.ajnanomat.com

Original Research Article

The drug delivery appraisal of Cu and Ni decorated $B_{12}N_{12}$ nanocage for an 8-hydroxyquinoline drug: A DFT and TD-DFT computational study

Hourinaz Darougari, Mahdi Rezaei-Sameti*

Department of Applied Chemistry, Faculty of Science, Malayer University, Malayer, 65174, Iran

ARTICLE INFORMATION

Received: 30 May 2022
Received in revised: 23 July 2022
Accepted: 31 July 2022
Available online: 9 August 2022

DOI: 10.26655/AJNANOMAT.2022.3.3

KEYWORDS

$B_{12}N_{12}$
Cu and Ni decorated
8-HQ drug
TD-DFT
RDG

ABSTRACT

In the current work, the density functional theory (DFT) and time-dependent density functional theory (TD-DFT) at ωB97XD/Lanl2DZ level of theory was accomplished to study the effects of Cu and Ni decorated on Boron nitride nanocage ($B_{12}N_{12}$) on the interaction of 8-hydroxyquinoline (8-HQ) drug as a novel candidate for drug delivery. The adsorption energy and thermodynamic results demonstrated that the adsorption of 8-HQ drug from O and N sites on the surface of nanocage was more favorable than other sites, and with decorating Cu and Ni atoms, the adsorption process of the 8-HQ drug was exothermic and spontaneous on the nanocage surface. The gap energy and global hardness values of the Ni and Cu decorated $B_{12}N_{12}$ nanocage was smaller than the pristine $B_{12}N_{12}$ nanocage, so the conductivity and reactivity of nanocage in this state was more than that the other states. The atom in molecule (AIM), reduced density gradient plots (RDG), and electron localized function (ELF) results confirmed that the nature of bonding between 8-HQ drugs with $B_{12}N_{12}$ nanocage was partially covalent or electrostatic. The UV-visible results revealed that with decorating Cu and Ni atoms, the optical properties of the system alter significantly from pure state. The results of this study can be used to make a novel sensitive sensor and novel drug delivery carriers for the 8-HQ drug..

© 2022 by SPC (Sami Publishing Company), Asian Journal of Nanoscience and Materials, Reproduction is permitted for noncommercial purposes.

Graphical Abstract

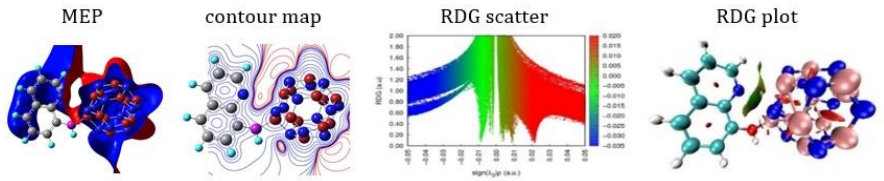

Corresponding author, email: mrsameti@malayeru.ac.ir (M. Rezaei-Sameti).
Tel.: +988132355404.

Introduction

In recent years, one of the most important challenges of the drug industry is to increase the therapeutic efficacy of the drug and deliver it accurately and completely to the target cells in the body. Various methods and combinations have been used to solve this issue. One of the newest methods is to use safe nanoparticles to deliver the drug to the target cells. Among the studied nanomaterials, Boron nitride nanocage ($B_{12}N_{12}$) has received more attention due to the physical and chemical properties, nonlinear optical features, oxidation resistance, inherent no cytotoxicity, and its wide application in the construction of electrical, magnetic, and imaging systems [1–6]. The theoretical results of Seifert *et al*. [7] demonstrated that $B_{12}N_{12}$ is more stable than other BN nanocages such as $B_{16}N_{16}$ and $B_{28}N_{28}$ nanocages and it is suitable for various interactions.

In 2004, Oku and coworker [8] were able to experimentally synthesize the $B_{12}N_{12}$ nanocage and identify it by mass spectroscopic methods. They showed that the $B_{12}N_{12}$ nanocage is composed of tetragonal and hexagonal rings and is semiconductor. The recent researches showed that the $B_{12}N_{12}$ has a high potential for adsorbing and interacting various compounds.

The interaction of $B_{12}N_{12}$ nanocage with NH_3 [9], carbon monoxide [10–12], carbon dioxide [13], nitrogen dioxide, nitrogen monoxide, and methane [14–16], hydrogen and hydrogen sulfide [17–19], hydrogen cyanide [20], tabun molecule [21], cyanogen halides [22], formic Acid [23], O_3 and SO_2 [24], hydrogen abstraction of methanimine [25], Methanol [26], methylamine [27], phosgene [28–29], pyridine [30], pyrrole [31], SCN^-[32], sulfur mustard chemical [33], halogen molecules [34], and Methanol dehydrogenation [35] were investigated through theoretical computational methods. The results of these studies demonstrated that the $B_{12}N_{12}$ nanocage has an excellent performance in adsorbing and characterizing these compounds in the environment and system. Moreover, extensive research has been conducted in the field of drug interaction with $B_{12}N_{12}$ nanocage, which is very important in the process of targeted drug delivery and the preparation of a drug-selective sensor. Abdolahi *et al.* [36] found that the interaction of the celecoxib drug with $B_{12}N_{12}$ nanocage is non-covalent and this nanocage is a good candidate for delivery and carrier of celecoxib drug. On the other study Soltani *et al.* [37] indicated that the interaction $B_{12}N_{12}$ nanocage with 5AVA drug is exothermic and $B_{12}N_{12}$ nanocage is a useful compound for delivery of 5AVA drug. Zhu *et al.* [38] computational results confirmed that the interaction of 5-aminosalicylic acid drug with $B_{12}N_{12}$, Al $B_{11}N_{12}$, and $GaB_{11}N_{12}$ nanocage is electrostatic and doped atoms (Al and Ga) increase the interaction drug with nanocage. In another study, Farmanzadeh *et al.* [39] displayed that the adsorption of amantadine drug on $B_{12}N_{12}$ nanocage in both gas and solvent is chemically type. Vessally *et al.* [40] reported that the Al doped $B_{12}N_{12}$ nanocage has a more potential for delivery and carrier of aspirin drug in bio systems. The 8-hydroxyquinoline (8-HQ) drug is widely used for the treatment of neuroprotection, anticancer, anti-HIV, antibacterial, and antifungal. The 8-HQs drug has shown interesting properties as a fungicide, bactericide antituberculosis agents, antineoplastic activity, metal-related diseases, and ant proliferative [41–45]. Following our previous works [46–55], in this project, we intend to study the interaction and adsorption of 8-HQ drug with pristine, Cu and Ni decorated $B_{12}N_{12}$ nanocage to evaluate its efficiency in identifying the drug and its delivery properties. By using the outputs of this study, it can be

suggested the sensitive sensors or delivery for 8-HQs drug.

Details of computational method

In the current study, the pristine, Ni and Cu decorated $B_{12}N_{12}$ nanocage are denoted with **A**, **B,** and **C** notation. The activated sites of 8-HQ drug adsorption on the nanocage surface are determined by **a** (for O site), and **b** (for N site) symbol (see Figure 1).

First, all possible complexes are considered for adsorbing 8-HQ drug on the surface of the $B_{12}N_{12}$, Ni, and Cu& $B_{12}N_{12}$ nanocages (see Figure 1), and all above complexes are optimized at ωB97XD/Lanl2DZ level of density functional theory (DFT) by using Gaussian 09 package [56]. The frequency analysis demonstrated that there was no imaginary frequency for these compounds. The optimization criteria for all studied complexes are Max Force=0.00038 Hartree and Max displacement=0.00015 Bohr. By applying equations of 1–4 the adsorption energy (E_{ads}), ΔG, ΔH, and ΔS for all complexes of 8-HQ drug with the $B_{12}N_{12}$, Cu, and Ni& $B_{12}N_{12}$ nanocages are calculated, as listed in Table 1.

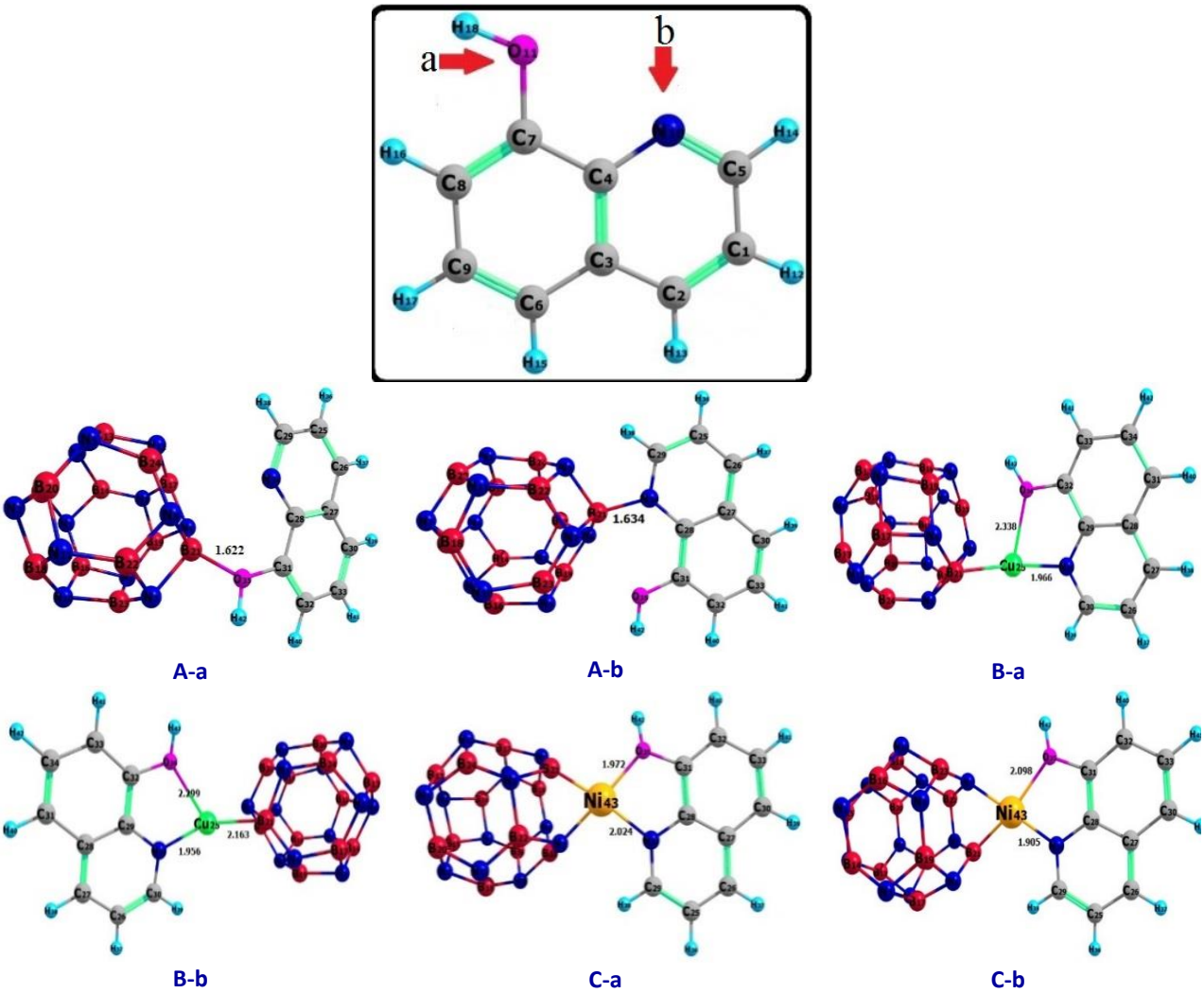

Figure 1. All complexes of 8-HQ with $B_{12}N_{12}$, Cu& $B_{12}N_{12}$, and Ni& $B_{12}N_{12}$ nanocages named with A-a to C-b complexes

Table 1. Adsorption energy (E_{ads}), thermodynamic parameters of 8-HQ with $B_{12}N_{12}$, Cu& $B_{12}N_{12}$, and Ni& $B_{12}N_{12}$ nanocages for A-a to C-d complexes

	$d_{(bond)}$ (Å)	E_{ads} (kcal/mol)	ΔG (kcal/mol)	ΔH (kcal/mol)	ΔS (kcal/mol.K)
A-a	1.62	-23.28	-9.28	-21.59	-0.041
A-b	1.63	-40.66	-25.04	-38.59	-0.045
B-a	1.96	-41.22	-27.55	-39.97	-0.042
B-b	2.16	-40.03	-27.48	-38.84	-0.038
C-a	1.97	-54.90	-39.91	-52.89	-0.043
C-b	1.91	-61.18	-46.44	-59.24	-0.043

$$E_{ads} = E_{8-HQ/nanocage\,complex} - (E_{nanocage} + E_{8-HQ}) \quad (1)$$

$$\Delta G = G_{8-HQ/nanocage\,complex} - (G_{nanocage} + G_{8-HQ}) \quad (2)$$

$$\Delta H = H_{8-HQ/nanocage\,complex} - (H_{nanocage} + H_{8-HQ}) \quad (3)$$

$$\Delta S = S_{8-HQ/nanocage\,complex} - (S_{nanocage} + S_{8-HQ}) \quad (4)$$

Where, the $E_{8\text{-}HQ\ /nanocage\ complex}$, $G_{8\text{-}HQ/nanocage\ complex}$, $H_{8\text{-}HQ/nanocage\ complex}$, and $S_{8\text{-}HQ/nanocage\ complex}$ are the total electronic energy, Gibbs free energy, enthalpy, and entropy of 8-HQ drug with pristine, Cu, and Ni decorated $B_{12}N_{12}$ nanocage complex, respectively. The $E_{8\text{-}HQ}$, $E_{nanocage}$, $G_{8\text{-}HQ}$, $G_{nanocage}$, $H_{8\text{-}HQ}$, $H_{nanocage}$, $S_{8\text{-}HQ}$, and $S_{nanocage}$ are the total electronic energy, Gibbs free energy, enthalpy, and entropy of isolated 8-HQ drug, pristine, or Cu and Ni decorated $B_{12}N_{12}$ nanocage, respectively. The base set superposition error values for all complexes is in the range 0.005–0.021 eV. The HOMO-LUMO energies, DOS plots, gap energy, electrochemical potential, global hardness, and total charge transfer parameter [57–61] for all drugs and nanocage complexes are estimated (see Table 2). The bonding nature between drug and nanocage can be determined by reduced density parameters (RDG), molecular electrostatic potential (MEP), and atoms in molecules (AIM) theory.

Results and Discussion

The geometrical, and adsorption parameters

The optimized geometrical structures of interaction 8-HQ drug from N, O, C2, and C6 sites with $B_{12}N_{12}$, Ni, and Cu & $B_{12}N_{12}$ nanocages are displayed in Figure 1, as it can be seen the interaction of 8-HQ drug from electrostatic sites (N and O) is more probable than C2 and C6 sites. The bond distance (d) between 8-HQ… nanocage at the A-a and A-b models are 1.62 and 1.63 Å. It is noticeable that with decorating Cu and Ni atoms, 8-HQ drug bind to the metal surface simultaneously from nitrogen and oxygen sites, moreover the Ni atom attaches to the B and N atoms of the $B_{12}N_{12}$ nanocage. The B–N bond lengths for tetragonal and hexagonal rings of $B_{12}N_{12}$ nanocage are 1.434 to 1.510 Å, respectively, and it is in agreement with other reports [3–6]. The stable site for adsorbing 8-HQ and decorating Cu and Ni atoms is B21 site. The bond lengths B21-N6, and B21-N7 in the pristine (**A**), Cu decorated (**B**), and Ni decorated (**C**) is 1.434 (1.510), 1.459 (1.637), and 1.448(1.602) Å, respectively. The B21-N6, and B21-N7 bond length in the A-a, A-b, B-a, B-b, C-a, and C-b complexes are (1.492, 1.607 Å), (1.521, 1.595 Å), (1.475, 1.757 Å), (1.482, 1.734 Å), (1.469, 1.895 Å), and (1.467, 1.900 Å), respectively. As you can see with decorating Ni

and Cu atoms, the bond length of B21-N7 alters sharply and so the electrical properties of the complex change significantly. These results suggest that Ni and Cu atoms play a catalytic role in this process and increase drug-nanocage interaction.

The E_{ads} values of all studied complexes (Table 1) are negative and exothermic.

The trend of increasing E_{ads} in models **a**, and **b** is as follows: C-a (−54.90 Kcal/mol)> B-a (−41.22 Kcal/mol)> A-a (−23.28 Kcal/mol), and C-b (−61.18 Kcal/mol)> B-a (−40.66 Kcal/mol)> A-a (−40.03 Kcal/mol). As result, the C-b adsorption complex is the most favorable, and Ni decorated plays a very good role in the adsorption process. By examining the results of thermodynamic parameters, it is observed that the ΔG and ΔH values of the A-a to C-b complexes are negative, and process spontaneous in a thermodynamic approach. Comparisons of the thermodynamic parameters values confirmed that the interaction of 8-HQ drug with Ni & $B_{12}N_{12}$ nanocage is the most favorable. Therefore, the Ni & $B_{12}N_{12}$ nanocage can be an appropriate suggestion for targeted delivery 8-HQ drug in the body. From output of thermodynamic calculation, the IR spectrum of all studied complexes is calculated and is displayed in Figure S3 (Supplementary data). In the IR spectrum of studied complexes, a sharp peak with high absorption intensity in the 1400−1500 cm^{-1} is observed for C−N bond stretching, and another peak has lower intensity.

HOMO and LUMO

To investigate the electrical behavior of the 8-HQ drug & $B_{12}N_{12}$ nanocage complex, the structures of HOMO and LUMO orbitals along with quantum parameters are calculated and the results are presented in Figure 2 and Table 2.

Figure 2 displays that in the Cu decorated $B_{12}N_{12}$ nanocage, the orbital structures of HOMO and LUMO of 8-HQ drug & $B_{12}N_{12}$ nanocage complex is separated into α and β spin due to the alone electron of valance layer of Cu. In the HOMO-LUMO orbitals figures, it can be seen that the highest HOMO density is concentrated on the nanocage surface, so this surface is more suitable for attacking electrophilicity species. While the highest LUMO density is concentrated on the 8-HQ drug surface, this area is suitable for a nucleophilicity attack. On the other hand, in the cellular environment, the drug part tends more towards negatively charged particles, while the nanocage tends towards to positively charged particles. This factor may play an important role in drug behavior therapy.

According to Table 2, the amount of E_{gap} values are in range of 1.353 to 4.235 eV. Therefore, with adsorbing 8-HQ drug and decorating Cu & Ni atoms, the conductivity of $B_{12}N_{12}$ nanocage enhances. This result suggests that the Cu & Ni decorated $B_{12}N_{12}$ nanocage can be a sensitive sensor for the 8-HQ drug. The E_{gap} amount for the alpha spin of B-a, and B-b models is lower than other models. Global hardness (η) is one of the useful parameters that can be used for determine the activity of a compound. The smaller values of η indicate that the compound is more active. This result indicates that the activity of 8-HQ drug with Ni & $B_{12}N_{12}$ nanocage complex is more than other studied systems. Thus, this property is more appropriate in the drug delivery phenomenon and therapeutic properties. The values of electrochemical potential for A-a to C-b complexes are negative and all studied complexes are stable in thermodynamic viewpoint. On the other hand, the ΔN and ρ_{NBO} values are positive, as result 8-HQ drug has a donor electron role in this system. The density of states (DOS) and partial density of state plots

of studied complexes are determined by GaussSum software, as displayed in Figure 3.

In the DOS plots, it is shown that with decorating Cu and Ni atoms, the number and intensity of peaks is more that pristine $B_{12}N_{12}$ nanocage, which indicates that the optical property of the system increase. Due to appearing a small peak in the gap area the E_{gap} of drug and nanocage complexes decrease from a pure state. The PDOS plots reveal that the highest interaction of the orbitals occur in the HOMO region. In the A-a, B-a, A-b, and B-b models, models the most interaction in HOMO region is observed for 2p orbital of C and N atoms of 8-HQ drug with N atoms of nanocage, while the interaction of the 3p orbital of C, N, and O atoms of the 8-HQ drug with B atoms of nanocage in the LUMO region is more than other atoms. In C-a and C-b models, in the HOMO and LUMO regions, the most interaction is observed between 2p and 3p orbitals of N and C atoms of drug with the same orbitals of nanocage atoms.

AIM analyses

The theory atom in molecule of the Bader [62] is one of the most important and practical techniques that is applied to determine the nature of binding between various materials. By using AIM theory the ρ, H_{BCP}, V_{BCP}, G_{BCP}, and $\nabla^2\rho(r)$, at the bond critical point of 8-HQ drug with $B_{12}N_{12}$ and Cu&$B_{12}N_{12}$, Ni&$B_{12}N_{12}$ nanocage complexes are calculated and outcomes are reported in Table 3. Based on the AIM theory, the strong covalent bond is indicated with $\nabla^2\rho(r) < 0$ and $H_{BCP} < 0$ values, the strong electrostatic bond is displayed with $\nabla^2\rho(r) > 0$ and $H_{BCP} > 0$ values, and partially covalent bond is determined with $H_{BCP} < 0$ and $\nabla^2\rho(r) > 0$ values [63–65].

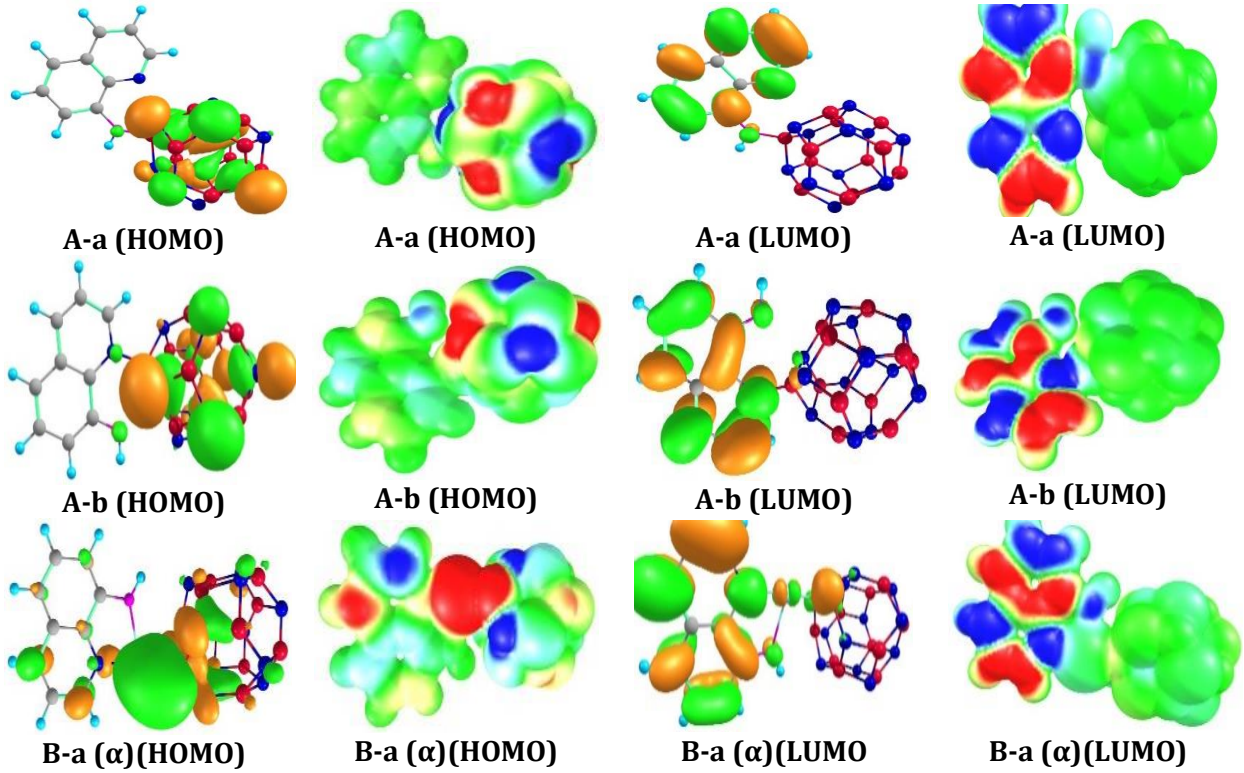

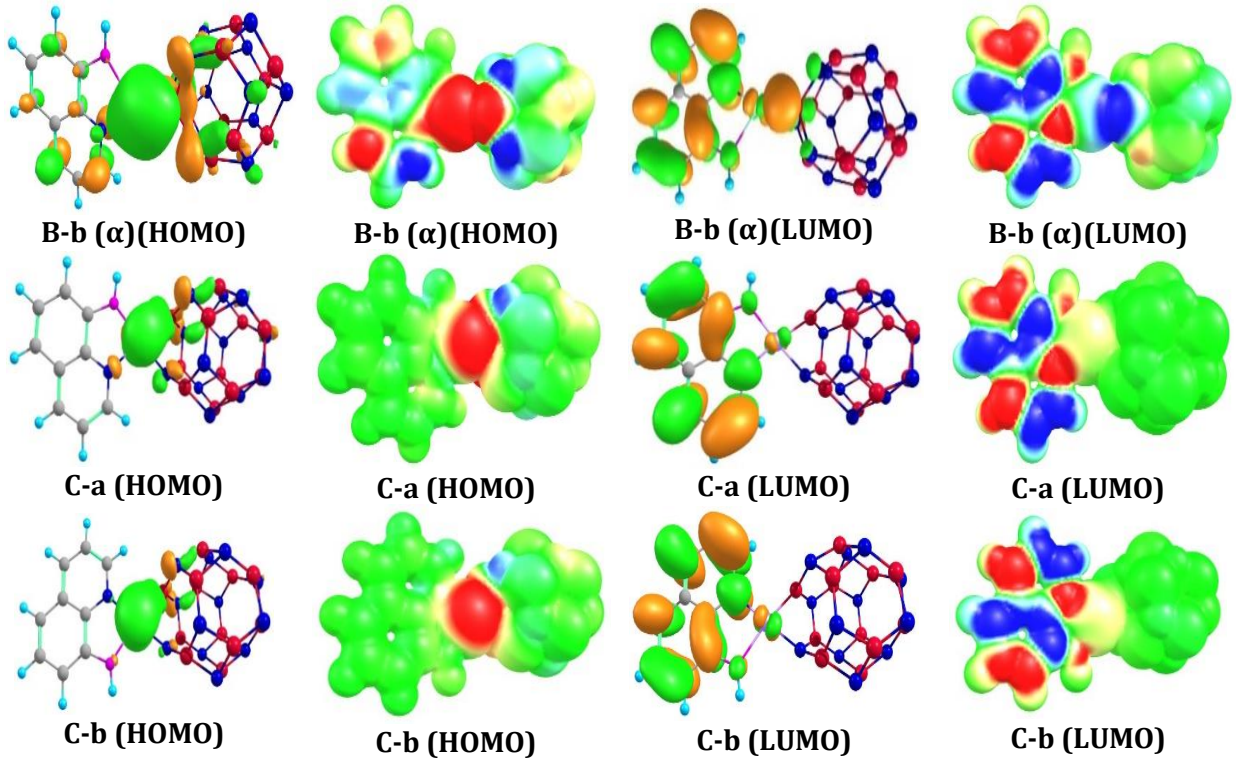

Figure 2. HOMO-LUMO orbital structures for A-a to C-b complexes

Table 2. Quantum parameters of 8-HQ with $B_{12}N_{12}$, Cu& $B_{12}N_{12}$, and Ni& $B_{12}N_{12}$ nanocages for A-a to C-d complexes

	E_{LUMO}/eV	E_{HOMO}/eV	E_{gap}/eV	η/eV	μ/eV	NΔ
A-a	-2.548	-6.787	4.238	2.119	-4.668	2.202
A-b	-3.220	-6.545	3.325	1.662	-4.882	2.936
B-a	-2.758	-4.209	1.450	2.830	-3.484	1.231
	-2.751	-6.594	3.843	1.921	-4.672	2.431
B-b	-2.704	-4.057	1.353	2.705	-5.409	1.999
	-2.652	-6.654	4.001	2.000	-4.653	2.325
C-a	-2.859	-5.527	2.667	1.333	-4.193	3.145
C-b	-2.871	-5.574	2.702	1.351	-4.222	3.125

(E_g= E_{LUMO}−E_{HOMO}), (μ= (E_{HOMO}+E_{LUMO})/2), (η= (E_{LUMO}−E_{HOMO})/2), and (ΔN= −μ/η)

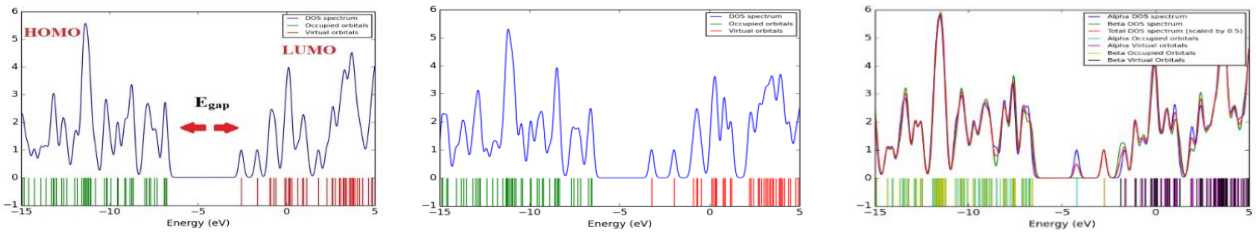

A-a **A-b** **B-a**

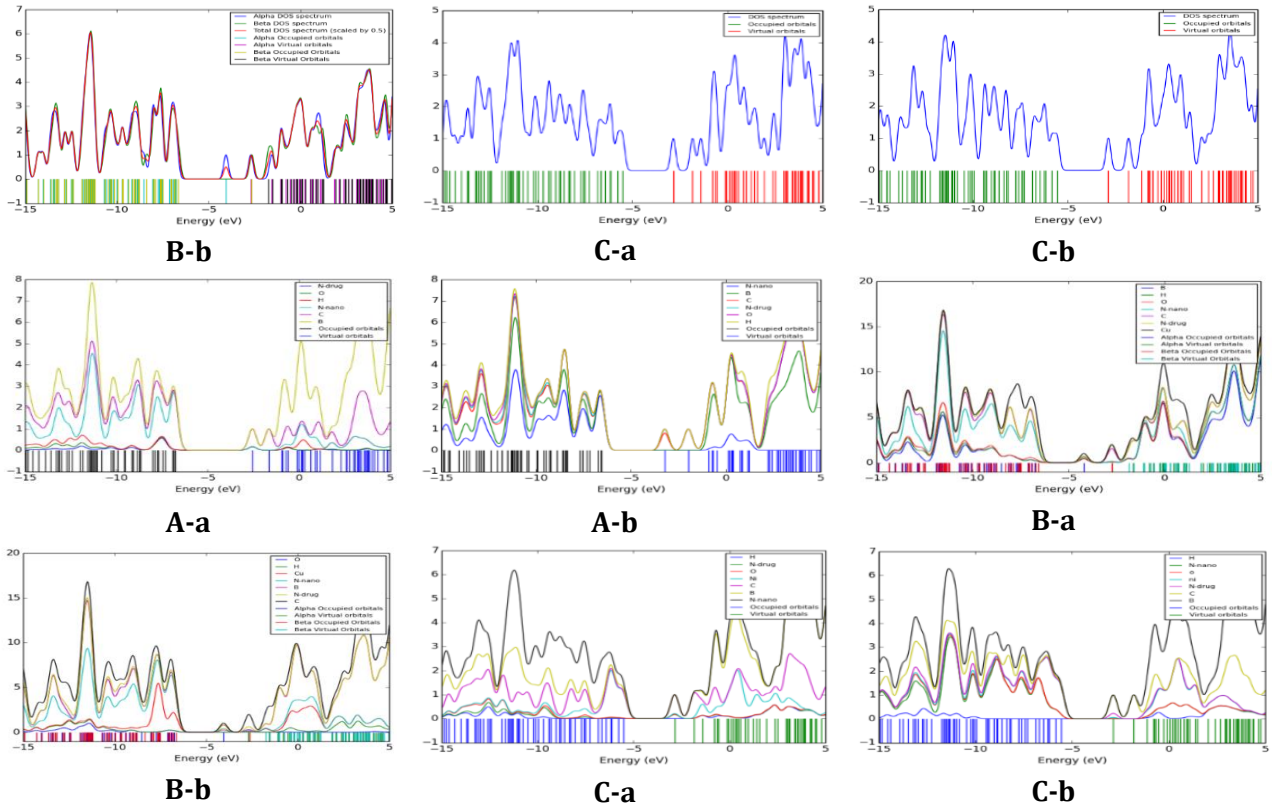

Figure 3. DOS and PDOS plots for A-a to C-b complexes

Table 3. Topological parameters of AIM of 8-HQ with $B_{12}N_{12}$, Cu& $B_{12}N_{12}$, and Ni& $B_{12}N_{12}$ nanocages for A-a to C-d complexes

	ρ	$\nabla^2\rho$	$H_{(r)}$	$V_{(r)}$	$G_{(r)}$	$-G_{(r)} / V_{(r)}$	ELF
A-a	0.090	0.364	-0.046	-0.184	0.137	0.745	0.125
A-b	0.080	0.311	-0.016	-0.110	0.094	0.854	0.173
B-a	0.165	0.231	-0.148	-0.354	0.206	0.582	0.326
B-b	0.188	0.309	-0.176	-0.430	0.254	0.591	0.327
C-a	0.266	-0.864	-0.257	-0.299	0.241	0.806	0.983
C-b	0.188	0.310	-0.177	-0.432	0.255	0.590	0.327

The calculated results of Table 3 revealed that the values of $\nabla^2\rho(r)$ and H_{BCP} for all adsorption models except the C-a model are positive and negative, respectively. Thus, the interaction of 8-HQ drug with $B_{12}N_{12}$ and Cu & $B_{12}N_{12}$, Ni & $B_{12}N_{12}$ nanocage complexes except C-a model is a partially covalent bond type. In the C-a model, the $\nabla^2\rho(r)$ and H_{BCP} values are negative, so the interaction between drug and nanocage is strong covalent bond. ELF (Electron localization function) is another functional parameter in which the determination of the electrons' concentration in the region between two compounds. If its value is less than 0.5 it indicates delocalization electron between two compounds and type of bonding is partial covalent, and if it is between 0.5 to 1, it indicates a localization electron between two compounds and nature of bonding is covalent. Examination of the results shows that the ELF value for all models except C-a model is less than 0.5 and the nature of the bond is partial covalent or

electrostatic type and for C-a model is greater than 0.5 and indicates the nature of the covalent bond.

RDG scatter plots

$$RDG(r) = \frac{1}{2(3\pi^2)^{1/3}} \frac{|\nabla\rho(r)|}{\rho(r)^{4/3}} \quad (5)$$

In this scatter diagram, the product of sign of λ_2 and ρ(r) (electron density) is applied to determine the different types of interactions between two compounds. The RDG scatter graphs for A-a to C-b complexes are determined, as depicted in Figure 4.

In the RDG scatter graphs, the blue (λ_2<0), green (λ_2=0) and red (λ_2 >0) colors indicate the attractive, van der Walls, and repulsive interactions. A close inspection of the RDG scatter graphs reveal that the RDG density for all studied complex is shown in the blue (λ_2<0) region. Therefore, the interactions between 8-HQ drug with nanocage is electrostatic or hydrogen bond type. The most density of RDG in the red (λ_2 >0) is related to the steric effects between O and N atoms of 8-HQ drug with nanocage. The analysis of RDG graphs confirms that the interaction of 8-HQ drug with $B_{12}N_{12}$, Cu&$B_{12}N_{12}$, and Ni& $B_{12}N_{12}$ nanocages except C-a model is electrostatic type.

MEP plots

A valuable method to study the charge distributions and nucleophilic or electrophilic properties of molecule is MEP [67]. In the MEP plots, red and blue colors indicate the nucleophilic (positive charge) and electrophilic (negative charge) of molecule surface, respectively.

To better understand the nature of non–covalent interaction between 8-HQ drug with $B_{12}N_{12}$ and Cu&$B_{12}N_{12}$, Ni& $B_{12}N_{12}$ nanocages, RDG (reduced density gradient) diagrams are very suitable that are extracted based on the following equation [66]:

According to the MEP plots in Figure 5, the positive charge is localized around the 8-HQ drug surface and this site is suitable for attacking to the negative site of biological cellule in the body. The decoration of Cu and Ni atoms alter the distribution of positive and negative charges around the drug and nanocage and cause the effect of drug on the target cell increase.

UV- visible spectrum

To understand of UV-visible spectrum and behavior of molecules in the exited state the TD-DFT calculated method is used at ωB97XD/Lanl2DZ level [68]. Thus, we considered 20 exited states to determine UV-visible spectra and transition states for all studied complexes. The UV-visible spectrums are displayed in Figure 6, and also the transition states parameters are listed in Table 4.

The values of the λ_{max} for A-a, and A-b complexes are demonstrated in the 282.01 and 234.78 nm with *f*=0.974 and 0.275 for transition states $S_0 \rightarrow S_5$ and $S_0 \rightarrow S_{30}$.

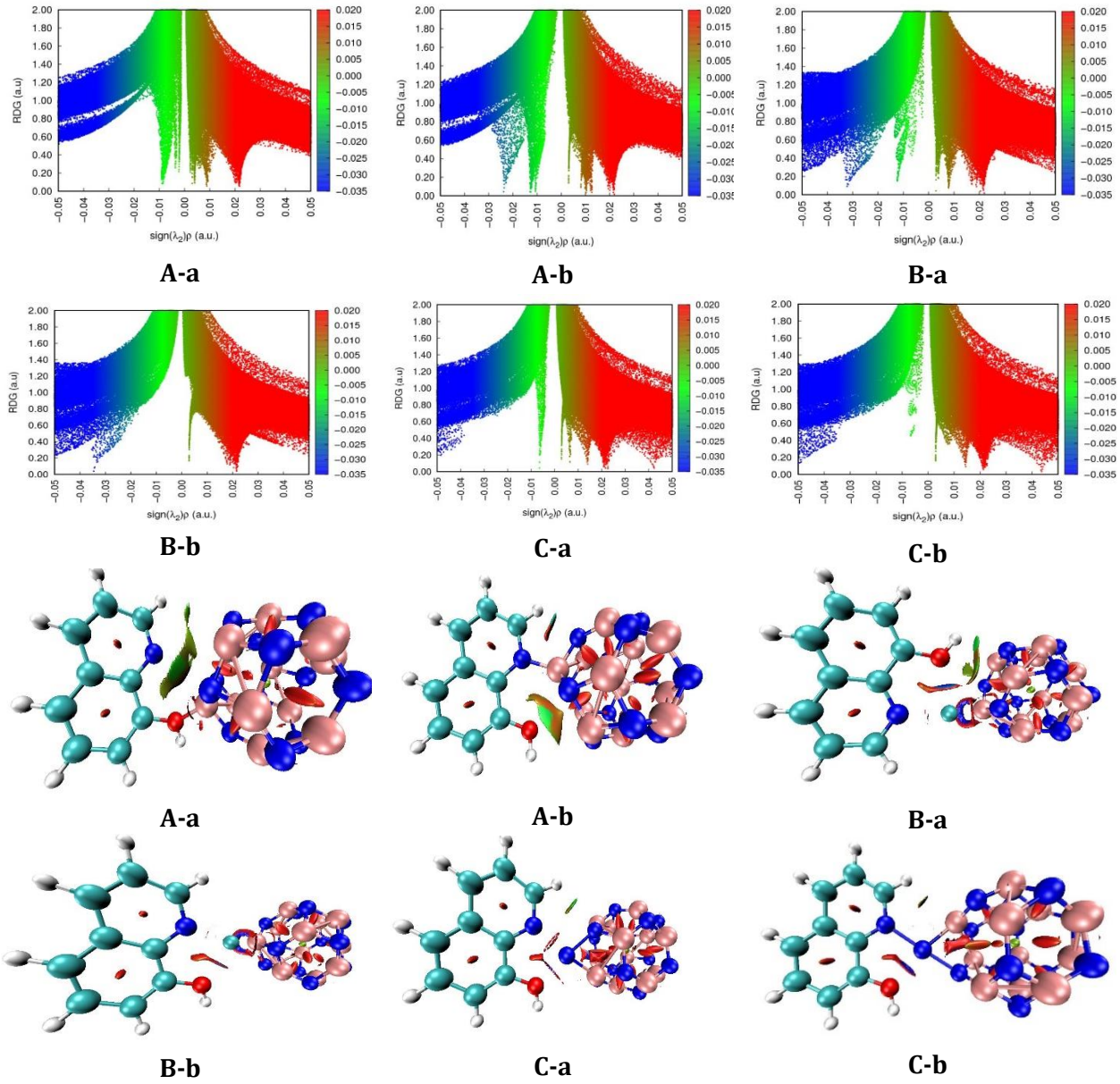

Figure 4. RDG scatter and plots for A-a to C-b complexes

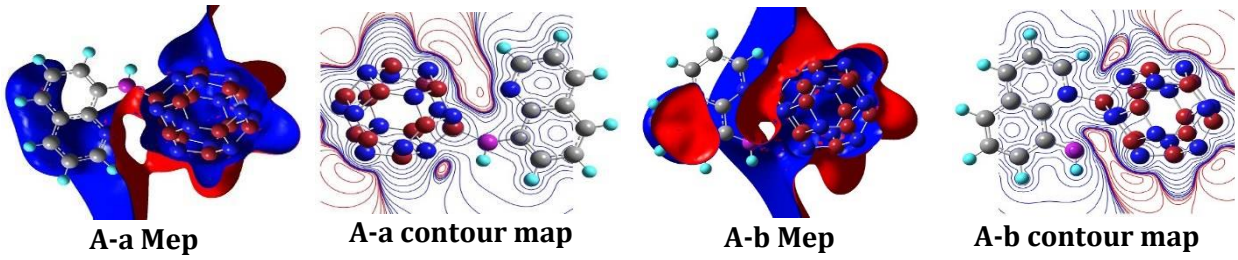

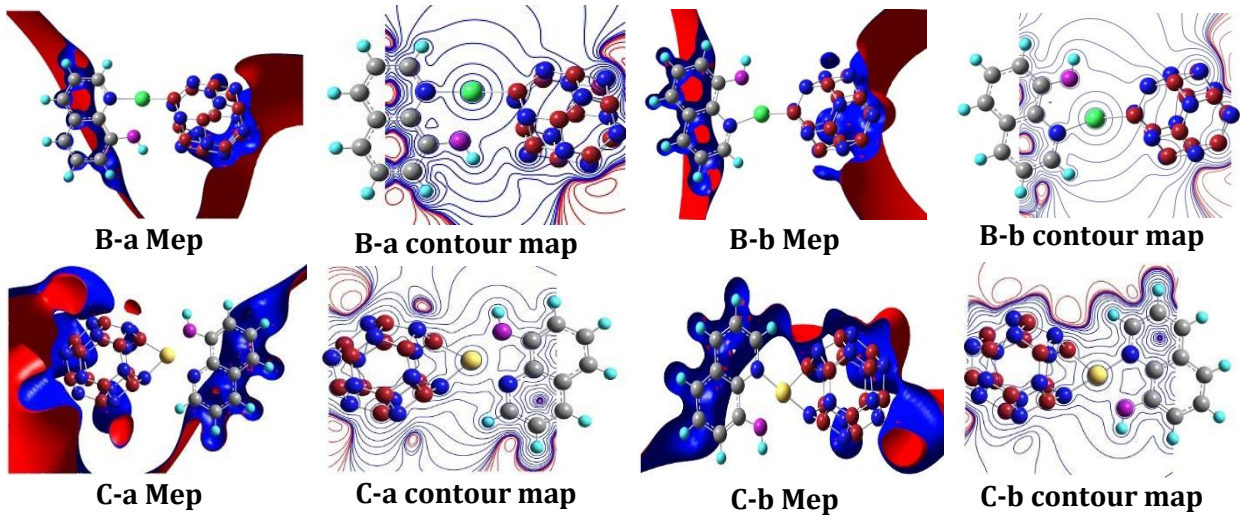

Figure 5. MEP plots for A-a to C-b complexes

Table 4. The exited energy of UV-visible parameters 8-HQ with $B_{12}N_{12}$, Cu & $B_{12}N_{12}$, and Ni & $B_{12}N_{12}$ nanocages for A-a to C-d complexes

Model	Exited	E_{xi} (eV)	λ (*nm*)	*f*	Configuration composite
A-a	**$S_0 \rightarrow S_5$**	4.396	282.01	0.9740	0.02(H-8→L)+0.03(H-8→L+1)+0.03(H-4→L) 0.85(H-3→L)
	$S_0 \rightarrow S_6$	4.5073	275.07	0.0107	0.41(H-8→L)-0.03(H-5→L)+0.04(H-3→L) +0.33(H-3→L+1)0.12(H→L+1)
A-b	**$S_0 \rightarrow S_4$**	3.4085	363.75	0.0554	0.95(H-3→L)
	$S_0 \rightarrow S_{30}$	5.28.09	234.78	0.2755	0.05(H-12→L)0.24(H-8→L)+0.22(H-6→L+1) -0.18(H-3→L+1)-0.13(H-1→L+5)
B-a	**$S_0 \rightarrow S_1$**	0.9800	1265.21	0.1076	1.99(H→L)
	$S_0 \rightarrow S_{13}$	3.2418	382.45	0.0377	-0.05 (H-2→L)+0.30 (H→L+6) -0.17 (H→L+7)-0.06 (H-3→L)-0.02 (H-3→L+1)+0.12 (H-1→L)+0.64 (H-1→L+1)-0.26 (H→L)
B-b	**$S_0 \rightarrow S_1$**	0.9856	1258.02	0.1703	2.02(H→L)-0.05(H→L)
	$S_0 \rightarrow S_{13}$	3.2743	378.65	0.0428	0.06(H-7→L)+0.02(H-6→L) +0.18(H-5→L) -0.28 (H-2→L)+0.18(H-1→L) +0.03(H→L+7)+0.02(H→L+8)+0.48(H→L+9)-0.02 (H→L+12)-0.25(H-1→L)+0.13(H→L+1)
C-a	**$S_0 \rightarrow S_6$**	2.6320	471.06	0.1011	0.55(H-3→L)-0.04(H-3→L+2)+0.22(H-2→L)-0.10(H-2→L+2)
	$S_0 \rightarrow S_{21}$	4.1513	298.67	0.0649	-0.02(H-9→L)+0.70(H-8→L)+0.149(H→L+6)
C-b	**$S_0 \rightarrow S_4$**	2.5952	477.75	0.0469	0.50(H-3→L)-0.25(H→L+2)-0.03 (H→L+3) +0.06(H→L+7)
	$S_0 \rightarrow S_{17}$	4.0004	309.93	0.0493	0.85(H-8→L)-0.03(H-4→L+1)-0.02(H→L+3)

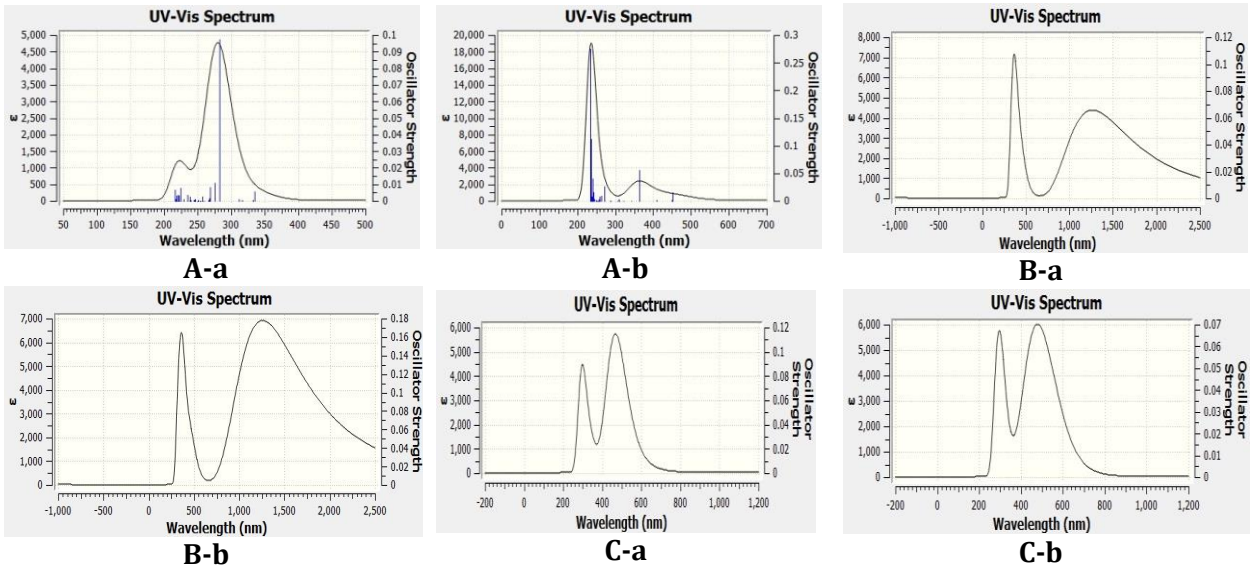

Figure 6. UV-visible plots for A-a to C-b complexes

While in the B-a and B-b complexes, a peak in the λ_{max} of 1265.21 and 1258.02 nm in *f*=0.1076 and 0.1703 is observed for transmissions $S_0 \rightarrow S_1$, and one peak is observed at the wavelengths of 382.48 and 378.65 nm with *f*=0.0377 and 0.0428 for transfers $S_0 \rightarrow S_{13}$ and $S_0 \rightarrow S_{13}$, respectively. The first peak is in the visible region and the second is in the ultraviolet region. With decorating Ni atom in the C-a, and C-b complexes, two peaks are also observed in the λ_{max} of 471.06 and 477.75 nm with *f*=0.1011 and 0.0469 for transfers $S_0 \rightarrow S_6$ and $S_0 \rightarrow S_4$, respectively. These peaks are in the visible area, and other peaks appear at 298.67 and 309.93 nm with *f* = 0.0649 and 0.0493 for transitions $S_0 \rightarrow S_4$ and $S_0 \rightarrow S_{17}$ are in the ultraviolet region. Therefore, with decorating of Cu and Ni atoms, the optical behavior of the 8-HQ drug and $B_{12}P_{12}$ nanocage complexes change significantly which is prominent in identifying the drug position in the body.

Conclusions

The interaction of 8-HQ drug with $B_{12}N_{12}$, Cu & $B_{12}N_{12}$, and Ni & $B_{12}N_{12}$ nanocages are investigated at the ωB97XD/Lanl2DZ level of DFT theory. The E_{ads} of the complex of 8-HQ drug with $B_{12}N_{12}$ and Cu & $B_{12}N_{12}$, Ni & $B_{12}N_{12}$ nanocages are exothermic and the trend of it as follows: C-a (-54.90 Kcal/mol)> B-a (-41.22 Kcal/mol)> A-a (-23.28 Kcal/mol), and C-b (-61.18 Kcal/mol)> B-a (-40.66 Kcal/mol)> A-a (-40.03 Kcal/mol). The E_{gap} and η values of 8-HQ drug and Cu and Ni atoms decorated $B_{12}N_{12}$ nanocage complexes are lower than pure states and the conductivity and reactivity of the complexes are more than the pure nanocage. The computational results of AIM, RDG, and ELF demonstrate that the bonding nature 8-HQ drug with $B_{12}N_{12}$, Cu & $B_{12}N_{12}$, and Ni & $B_{12}N_{12}$ nanocages is partially covalent or electrostatic. The TD-DFT results indicate that the optical properties of the 8-HQ drug with $B_{12}N_{12}$, Cu & $B_{12}N_{12}$, and Ni & $B_{12}N_{12}$ nanocages complexes alter significantly from pure state and this feature is remarkable for tracking the drug in the body. The computational results of this study suggest that Ni & $B_{12}N_{12}$ is an excellent carrier for targeted drug delivery to target cells.

Disclosure Statement

No potential conflict of interest was reported by the authors.

Funding

This research did not receive any specific grant from funding agencies in the public, commercial, or not-for-profit sectors.

Authors' contributions

All authors contributed to data analysis, drafting, and revising of the paper and agreed to be responsible for all the aspects of this work.

Supporting Information

Figures S1- S3 are depicted in supplementary data.

References

[1]. Evarestov R.A., Theoretical Modeling of Inorganic Nanostructures, Springer, 2015; p 835 [Crossref], [Publisher]

[2]. Baumeier B., Kruger P. *Phys. Rev. B,* 2007, **76**:085407 [Crossref], [Google Scholar], [Publisher]

[3]. Karamanis P., Pouchan C. *J. Phys. Chem. C.*, 2012, **116**:11808 [Crossref], [Google Scholar], [Publisher]

[4]. Tang C., Chen S., Zhu W., Zhang A., Zhang K., Liu M. *Eur. Phys. J. D.*, 2014, **68**:19 [Crossref], [Google Scholar], [Publisher]

[5]. Beheshtian J., Bagheri Z., Kamfiroozi M., Ahmadi A. *J. Mol. Model*, 2012, **18**:2653 [Crossref], [Google Scholar], [Publisher]

[6]. Golberg D., Bando Y., Huang Y., Terao T., Mitome, Tang C., Zhi C. *ACS Nano*, 2010, **4**: 2979 [Crossref], [Google Scholar], [Publisher]

[7]. Seifert G., Fowler R., Mitchell D., Porezag D., Frauenheim T. *Chem. Phys. Lett.*, 1997, **268**:352 [Crossref], [Google Scholar], [Publisher]

[8]. Oku T., Nishiwaki A., Narita I. *Sci. Technol. Adv. Mater.*, 2004, **5**:635 [Crossref], [Google Scholar], [Publisher]

[9]. Ahmadi A., Beheshtian J., Hadipour N.L. *Physica E.*, 2011, **43**:1717 [Crossref], [Google Scholar], [Publisher]

[10]. Vessallya E., Soleimani-Amiri S. *Physica E*, 2017, **87**:308 [Crossref], [Google Scholar], [Publisher]

[11]. Beheshtian J., Bagheri Z., Kamfiroozi M. *Microelec. J.* 2011, **42**:1400 [Crossref], [Google Scholar], [Publisher]

[12]. Vessally E., Soleimani-Amiri S. *Physica E.* 2017, **87**:308 [Crossref], [Google Scholar], [Publisher]

[13]. Baei M.T., Bagheri Z., Peyghan A.A. *Bull. Korean Chem. Soc.*, 2012, **33**:3338 [Google Scholar], [Publisher]

[14]. Beheshtian J., Kamfiroozi M., Bagheri Z., Peyghan A.A. *Chin. J. Chem. Phys.*, 2012, **25**:60 [Crossref], [Google Scholar], [Publisher]

[15]. Onsori S., Liyaghati-Delshad M. *Chem. Phys. Lett.*, 2017, **680**:22 [Crossref], [Google Scholar], [Publisher]

[16]. Beheshtian J., Peyghan A.A., Bagheri Z., Kamfiroozi M. *Struct. Chem.*, 2012, **23**:1567 [Crossref], [Google Scholar], [Publisher]

[17]. Shokuhi Rad A., Ayub K. *J. Hydrogen Energy*, 2016, **41**:22182 [Crossref], [Google Scholar], [Publisher]

[18]. Ghorbanzadeh Ahangari M., Hamed Mashhadzadeh A. *Inter. J. Hydrogen Energy*, 2020, **45**:6745 [Crossref], [Google Scholar], [Publisher]

[19]. Rahimi F., Zabaradsti A. *J. Inorg. Organomet. Polym.*, 2017, **27**:1770 [Crossref], [Google Scholar], [Publisher]

[20]. Baei M.T. *Comp. Theo. Chem.*, 2013, **1024**:28 [Crossref], [Google Scholar], [Publisher]

[21]. Fallahi P., Jouypazadeh H., Farrokhpour H. *J. Molecular Liq.*, 2018, **60**:138 [Crossref], [Google Scholar], [Publisher]

[22]. Vessally E., Behmagham F., Massuomi B., Hosseinian A., Nejati K. *J. Mol. Model.*, 2017, **23**:138 [Crossref], [Google Scholar], [Publisher]

[23]. Esrafili M.D., Nurazar R. *J. Clust. Sci*., 2015, **26**:595 [Crossref], [Google Scholar], [Publisher]
[24]. Shokuhi Rad A., Ayub K. *Solid. State. Sci.,* 2017, **69**:22 [Crossref], [Google Scholar], [Publisher]
[25]. Rahimi R., Solimannejad M. *Stru. Chem*., 2020, **31**:447 [Crossref], [Google Scholar], [Publisher]
[26]. Esrafili M.D., Nurazar R. *Superlat. Microstr*., 2014, **67**:54 [Crossref], [Google Scholar], [Publisher]
[27]. Esrafili M.D., Nurazar R. *Surface Sci*., 2014, **626**:44 [Crossref], [Google Scholar], [Publisher]
[28]. Shakerzadeh E., Khodayar E., Noorizadeh S. *Comp. Mat. Sci*., 2016, **118**:155 [Crossref], [Google Scholar], [Publisher]
[29]. Padash R., Rahimi-Nasrabadi M., Shokuhi Rad A., Sobhani-Nasab A., Jesionowski T., Ehrlich H. *J. Cluster. Sci*., 2019, **30**:203 [Crossref], [Google Scholar], [Publisher]
[30]. Baei M.T. *Superlat. Microstr*., 2013, **58**:31 [Crossref], [Google Scholar], [Publisher]
[31]. Shokuhi Rad A., Ayub K. *Vacuum.,* 2016, **131**:135 [Crossref], [Google Scholar], [Publisher]
[32]. Soltani A., Baei M.T., Tazikeh Lemeski E., Allah Pahlevani A. *Superlat. Microstr*., 2014, **75**:716 [Crossref], [Google Scholar], [Publisher]
[33]. Jouypazadeh H., Farrokhpour H. *J. Mole. Str.,* 2018, **1164**:227 [Google Scholar], [Publisher]
[34]. Bahrami A., Balooch Qarai M., Hadipour N. L. *Comp. Theo. Chem*., 2017, **1108**:63 [Crossref], [Google Scholar], [Publisher]
[35]. Esrafili M.D., Nurazar R. *Comp. Mat. Sci*., 2014,**92**:172 [Crossref], [Google Scholar], [Publisher]
[36]. Abdolahi N., Aghaei M., Soltani A., Azmoodeh Z., Balakheyli H., Heidari F. Spectrochim. Acta. Part. A. *Mol. Biomol. Spectrosc*., 2018, **204**:348 [Crossref], [Google Scholar], [Publisher]
[37]. Soltani A., Sousaraei A., Bezi Javan M., Eskandari M., Balakheyli H. *New J. Chem*., 2016, **40**:7018 [Crossref], [Google Scholar], [Publisher]
[38]. Zhu H., Zhao C., Cai Q., Fu X., Rashid Sheykhahmad F. *Inorganic Chem. Commun*., 2020, **114**:107808 [Crossref], [Google Scholar], [Publisher]
[39]. Farmanzadeh D., Keyhanian M., Theo. *Chem. Accounts.,* 2019, **138**:1 [Crossref], [Google Scholar], [Publisher]
[40]. Vessally E., Esrafili M.D., Nurazar R., Nematollahi P., Bekhradni A. *Struct. Chem*., 2017, **28**:735 [Crossref], [Google Scholar], [Publisher]
[41]. Zhai S., Yang L., Cui Q.C., Sun Y., Dou Q.P., Yan B. *J. Biol. Inorg. Chem*., 2010, **15**:259 [Crossref], [Google Scholar], [Publisher]
[42]. Prachayasittiku V., Prachayasittikul S., Ruchirawat S., Prachayasittikul V. *Drug Des. Develop. Therapy,* 2013, **7**:1157 [Crossref], [Google Scholar], [Publisher]
[43]. Zouhiri F., Danet M., Benard C., Normand-Bayle M., Mouscadet J.F., Leh H., Thomas C.M., Mbemba G., D'Angelo J., Desmaele G. *Tetrahedron Lett.,* 2005, **46**:2201 [Crossref], [Google Scholar], [Publisher]
[44]. Rasoul-Amini S., Khalaj A., Shafiee A., Daneshtalab M., Madadkar-Sobhani A., Fouladdel S., Azizi E. *Int. J. Cancer Res.,* 2006, **2**:102 [Google Scholar], [Publisher]
[45]. Musiol R., Serda M., Hensel-Bielowka S., Polanski J. *Current. Med. Chem*., 2010, **17**:1960 [Crossref], [Google Scholar], [Publisher]
[46]. Rezaei-Sameti M., Amirian B. *Asian J. Nanosci. Mater.*, 2018, **1**:262 [Google Scholar], [Publisher]
[47]. Rezaei-Sameti M., Zarei P. *Adsorption*, 2018, **24**:757 [Crossref], [Google Scholar], [Publisher]
[48]. Korivand N., Rezaei-Sameti M. *Asian J. Nanosci. Mater.*, 2019, **2**:399 [Crossref], [Google Scholar], [Publisher]

[49]. Rezaei-Sameti M., Abdoli S.K. *J. Mol. Stru.*, 2020, **1205**:127593 [Crossref], [Google Scholar], [Publisher]
[50]. Rezaei-Sameti M., Zanganeh H. *Phys. Chem. Res.*, 2020, **8**:511 [Crossref], [Google Scholar], [Publisher]
[51]. Rezaei–Sameti M., Jafari M. *Chem. Methodologies.*, 2020, **4**:494 [Crossref], [Google Scholar], [Publisher]
[52]. Rezaei-Sameti M. Rakhshi, *Mol. Phys.*, 2021, 1822556 [Crossref], [Google Scholar], [Publisher]
[53]. Alvand R., Rezaei-Sameti M. *Adsorption.*, 2021, **27**:91 [Crossref], [Google Scholar], [Publisher]
[54]. Rezaei-Sameti M., Khani H. *Phys. Chem.,* 2022, **10**: 89 [Google Scholar], [Publisher]
[55]. Mehraein G., Rezaei-Sameti M., Asgary E., Aghamohammadi M. *J. Mol. Stru.*, 2022, **1248**:131478 [Crossref], [Google Scholar], [Publisher]
[56]. Frisch M.J., *et al*. *GAUSSIAN 09*, Revision D.01, 2009 [Publisher]
[57]. Parr R.G., Szentpaly L.V., Liu S. *J. Am. Chem. Soc.*, 1999, **121**:1922 [Crossref], [Google Scholar], [Publisher]
[58]. Pearson R.G. *PNAS-USA*, 1986, **83**:8440 [Crossref], [Google Scholar], [Publisher]
[59]. Padmanabhan J., Parthasarathi R., Subramanian V., Chattaraj P.K., *J. Phys. Chem. A.*, 2007, **111**:1358 [Crossref], [Google Scholar], [Publisher]
[60]. Sarker Md. N., Jahidul Islam M., Paul S. *Asian J. Nanosci. Mater.*, 2019, **2**:439 [Crossref], [Google Scholar], [Publisher]
[61]. Godarzi M., Ahmadi R., Ghiasi R. *Asian J. Green. Chem.,* 2020, **4**:220 [Crossref], [Google Scholar], [Publisher]
[62]. Bader R.F.W. *Oxford University Press, Oxford, U.K.*, 1990 [Publisher]
[63]. Johnson E.R., Keinan S., Mori–Sanchez P., Contreras–Garcia J., Cohen A. J., Yang W. *J. Am. Chem. Soc.*, 2010, **132**:6498 [Crossref], [Google Scholar], [Publisher]
[64]. Bayat M., Yaghoobi F., Salehzadeh S., Hokmi S. *Polyhedron.*, 2011, **30**:2809 [Crossref], [Google Scholar], [Publisher]
[65]. Srivastava A., Mishra R., Kumar S., Dev K., Tandon P., Maurya R. *J. Mol. Struct.*, 2015, **1084**:55 [Crossref], [Google Scholar], [Publisher]
[66]. Lu T., Chen F. *J. Comput. Chem.*, 2012, **33**:580 [Crossref], [Google Scholar], [Publisher]
[67]. Bulat F.A., Burgess J.S., Matis B.R., Baldwin J.W., Macaveiu L., Murray J.S., Politzer P. *J. Phys. Chem. A.,* 2012, **116**:8644 [Crossref], [Google Scholar], [Publisher]
[68]. Sun Y.T., Huang P.Y., Lin C.H., Lee K.R., Lee M.T. *Biophys. J.*, 2015, **110**:414 [Google Scholar], [Publisher]

How to cite this manuscript: Hourinaz Darougari, Mahdi Rezaei-Sameti. The drug delivery appraisal of Cu and Ni decorated $B_{12}N_{12}$ nanocage for an 8-hydroxyquinoline drug: A DFT and TD-DFT computational study. *Asian Journal of Nanoscience and Materials*, 5(3) 2022, 196-210. DOI: 10.26655/AJNANOMAT.2022.3.3.